

The Resolution Sensitivity of Northern Hemisphere Blocking in Four 25-km Atmospheric Global Circulation Models

REINHARD SCHIEMANN, MARIE-ESTELLE DEMORY, LEN C. SHAFFREY,
JANE STRACHAN,^a AND PIER LUIGI VIDALE

National Centre for Atmospheric Science, Department of Meteorology, University of Reading, Reading, United Kingdom

MATTHEW S. MIZIELINSKI AND MALCOLM J. ROBERTS

Met Office Hadley Centre, Exeter, United Kingdom

MIO MATSUEDA

*Center for Computational Sciences, University of Tsukuba, Tsukuba, Japan, and Department of Physics,
University of Oxford, Oxford, United Kingdom*

MICHAEL F. WEHNER

Lawrence Berkeley National Laboratory, Berkeley, California


THOMAS JUNG

European Centre for Medium-Range Weather Forecasts, Reading, United Kingdom, and Alfred Wegener Institute, Bremerhaven, Germany


(Manuscript received 28 January 2016, in final form 12 September 2016)

ABSTRACT

The aim of this study is to investigate if the representation of Northern Hemisphere blocking is sensitive to resolution in current-generation atmospheric global circulation models (AGCMs). An evaluation is conducted of how well atmospheric blocking is represented in four AGCMs whose horizontal resolution is increased from a grid spacing of more than 100 km to about 25 km. It is shown that Euro-Atlantic blocking is simulated overall more credibly at higher resolution (i.e., in better agreement with a 50-yr reference blocking climatology created from the reanalyses ERA-40 and ERA-Interim). The improvement seen with resolution depends on the season and to some extent on the model considered. Euro-Atlantic blocking is simulated more realistically at higher resolution in winter, spring, and autumn, and robustly so across the model ensemble. The improvement in spring is larger than that in winter and autumn. Summer blocking is found to be better simulated at higher resolution by one model only, with little change seen in the other three models. The representation of Pacific blocking is not found to systematically depend on resolution. Despite the improvements seen with resolution, the 25-km models still exhibit large biases in Euro-Atlantic blocking. For example, three of the four 25-km models underestimate winter northern European blocking frequency by about one-third. The resolution sensitivity and biases in the simulated blocking are shown to be in part associated with the mean-state biases in the models' midlatitude circulation.

 Denotes Open Access content.

^a Current affiliation: Met Office Hadley Centre, Exeter, United Kingdom.

 Supplemental information related to this paper is available at the Journals Online website: <http://dx.doi.org/10.1175/JCLI-D-16-0100.s1>.



This article is licensed under a [Creative Commons Attribution 4.0 license](https://creativecommons.org/licenses/by/4.0/).

Corresponding author address: R. Schiemann, NCAS–Climate, Department of Meteorology, University of Reading, Earley Gate, P.O. box 243, Reading RG6 6BB, United Kingdom.
E-mail: r.k.schiemann@reading.ac.uk

DOI: 10.1175/JCLI-D-16-0100.1

1. Introduction

Blocking refers to the occurrence of quasi-stationary high pressure systems at midlatitudes and can be described by a number of key characteristics (Barriopedro et al. 2010); blocking highs persist for several days to weeks and often divert cyclones traveling in the storm track poleward or equatorward (Rex 1950; Woollings et al. 2010; Zappa et al. 2014). Preferred regions of blocking occurrence are the eastern sides of the Atlantic and Pacific Oceans. Blocks are observed throughout the year with a peak occurrence in winter and spring (Tibaldi et al. 1994). The persistent circulation during blocking episodes causes anomalous surface weather conditions and possibly extreme events. Recent examples include the cold European 2009/10 winter (Cattiaux et al. 2010) and the 2010 Russian heat wave (Barriopedro et al. 2011; Matsueda 2011; Otto et al. 2012).

Despite the lack of a single unified blocking theory, a number of detailed studies of the mechanisms responsible for blocking formation and maintenance have been conducted. Croci-Maspoli (2005) provides a brief overview of these studies and classifies them into theories based on low-frequency–planetary-scale and high-frequency–synoptic-scale dynamics. An example of the low-frequency class is the study by Charney and DeVore (1979). Using a quasigeostrophic zonal channel model, Charney and DeVore (1979) show that there are two equilibrium states for the topographically driven disturbances of a zonal flow, a flow with a strong wave component (blocked situation) and a flow with a stronger zonal component. In contrast to the low-frequency class, studies of the high-frequency class include high-frequency activity such as transient eddies in the vicinity of blocking formation and maintenance. These small-scale eddies are shown to be important for the maintenance of blocking (Shutts 1983, 1986) and for sustaining low-frequency flow in general (Kug and Jin 2009). Shutts (1983) shows that the eddies transfer energy to the larger-scale split-jet flow in a blocking situation and that the vorticity transport by the eddies can maintain blocking patterns against advection by the mean flow.

Both coupled and atmosphere-only general circulation models (GCMs) tend to underestimate the occurrence frequency and persistence of blocking events (D'Andrea et al. 1998; Boyle 2006; Anstey et al. 2013; Masato et al. 2013). These biases are long-standing, and the reasons for the models' shortcomings are not fully understood. Several studies have shown that increasing the horizontal resolution in an atmospheric model is beneficial for the representation of blocking in the Northern (e.g., Matsueda et al. 2009; Jung et al. 2012)

and Southern (Matsueda et al. 2010) Hemispheres, consistent with the notion that the better representation of small-scale eddies and orography (Berckmans et al. 2013) at higher resolution allows for a better simulation of blocking. Other authors have emphasized the importance of improved physical parameterizations (Jung et al. 2010) and of vertical model resolution (Anstey et al. 2013).

Moreover, different arguments have been put forward to interpret the improvement in blocking due to increased horizontal resolution. One possibility is that the simulation of blocking as a process can be thought to be sensitive to model resolution. Another possibility is that it is mainly the mean state of the model that is sensitive to resolution, and any improvement seen in the blocking climatology is largely a reflection of the improvement of the mean state due to higher resolution (Woollings 2010; Scaife et al. 2010). These two possibilities cannot be fully disentangled because of the interaction between the mean state and eddies. However, some insight into the relevance of the mean-state bias can be gained by correcting the mean bias in model data before the blocking identification is applied (Scaife et al. 2010).

A robust assessment of blocking biases in models requires ensembles of multidecadal simulations because of the large variability of blocking on interannual and longer time scales. This implies particular computational challenges when investigating the sensitivity to model resolution since the required sampling statistics need to be accumulated at the highest desired resolution. Therefore, investigations into the role of model resolution for blocking have relied either on the ensembles of opportunity offered, for example, by phase 5 of the Coupled Model Intercomparison Project (CMIP5; Anstey et al. 2013; Masato et al. 2013), or on the controlled increase of resolution in individual GCMs (Matsueda et al. 2009; Jung et al. 2012; Berckmans et al. 2013).

Recent advances in computing power and investment in higher model resolution have enabled several modeling centers to run atmospheric GCMs (AGCMs) at about 25-km grid spacing for the simulation lengths and ensemble sizes required for the evaluation of blocking in these higher-resolution climate models. These advances allow the question of the resolution sensitivity of blocking to be systematically revisited in a multimodel study. This study aims to use an ensemble of present-day climate simulations from four AGCMs with about 25-km grid spacing at midlatitudes to (i) quantify biases in the representation of blocking throughout the year and (ii) assess the sensitivity of these biases to the model resolution. Furthermore, we follow the method suggested by Scaife et al. (2010) to determine to what extent

TABLE 1. AGCMs used in this study.

Acronym	Model	Center	Vertical levels	References
CAM5	CAM5.1	National Center for Atmospheric Research (United States)	30	Neale (2012)
IFS	IFS (Athena)	European Centre for Medium-Range Weather Forecasts (United Kingdom)	91	Jung et al. (2012) and Kinter et al. (2013)
MRI	MRI-AGCM3.2	Meteorological Research Institute (Japan)	64	Mizuta et al. (2012)
UM	HadGEM3-GA3.0	Met Office Hadley Centre (United Kingdom)	85	Walters et al. (2011)

any blocking bias and resolution sensitivity are associated with the mean-state bias of the models.

The outline of this paper is as follows: [section 2](#) describes the blocking identification method, the models and model experiments, and the reference reanalysis data against which we perform model evaluation. [Section 3](#) illustrates the blocking climatology in reanalysis data, and thereafter the main results of this study regarding model performance and resolution sensitivity are presented in [section 4](#). [Section 5](#) assesses the role of mean-state biases, and the paper is concluded in [section 6](#).

2. Methods, models, and data

a. Model ensemble and reanalyses

This study is based on an ensemble comprising high-resolution AGCM simulations conducted independently at four different modeling centers. The four models are the Community Atmospheric Model (CAM5.1), the European Centre for Medium-Range Weather Forecasts (ECMWF) Integrated Forecasting System (IFS), the Meteorological Research Institute model (MRI-AGCM3.2), and the Met Office Hadley Centre Global Environmental

Model (HadGEM3-GA3.0). [Table 1](#) provides an overview of the four models and corresponding references, and [Table 2](#) shows the simulations that have been conducted with each model. For all four models, these experiments are designed to test the sensitivity of the simulated climate to horizontal resolution only (i.e., retuning at the different resolutions has been kept to a minimum; see, e.g., discussion in [Demory et al. 2014](#)). Blocking climatologies are calculated for the full simulation period of each model ([Table 2](#)) and evaluated against a 50-year reanalysis climatology (see also [section 3](#)).

The ECMWF retrospective analyses ERA-40 and ERA-Interim are used to evaluate the model simulations. Additionally, blocking in these two reanalyses is compared with that in NASA's Modern-Era Retrospective Analysis for Research and Applications (MERRA) to assess the agreement of different reanalyses on blocking climatologies. The three reanalyses are overviewed in [Table 3](#).

b. Blocking identification

We follow the blocking identification method used by [Scherrer et al. \(2006\)](#) using the absolute geopotential height (AGP) index. The AGP index is an extension of

TABLE 2. Model experiments. Grid spacings are given at 50°N for CAM5 and UM (square root of gridbox area and zonal × meridional spacing in parentheses). IFS and MRI are spectral models. The sea surface temperature (SST) forcing datasets are monthly Atmospheric Model Intercomparison Project phase I (AMIP I; [Gates 1992](#)), three different SST products for the Athena IFS simulations (see [Jung et al. 2012](#) for details), monthly HadISST1 ([Rayner et al. 2003](#)), and daily Operational Sea Surface Temperature and Sea Ice Analysis (OSTIA) forcing ([Donlon et al. 2012](#)).

Model	Resolution	Grid spacing (km)	Ensemble (size × years)	Period	SST forcing
CAM5	$1.3^{\circ} \times 0.9^{\circ}$	96 (93 × 100)	3 × 27	1979–2005	AMIP I
CAM5	$0.31^{\circ} \times 0.23^{\circ}$	24 (22 × 26)	1 × 27	1979–2005	AMIP I
IFS	T159	126	1 × 46	1962–2007	Athena
IFS	T1279	16	1 × 46	1962–2007	Athena
MRI	T95	208	4 × 25	1979–2003	HadISST1
MRI	T319	63	4 × 25	1979–2003	HadISST1
MRI	T959	21	2 × 25	1979–2003	HadISST1
UM	N96	136 (134 × 139)	5 × 26	1986–2011	OSTIA
UM	N216	61 (60 × 62)	3 × 26	1986–2011	OSTIA
UM	N512	26 (25 × 26)	5 × 26	1986–2011	OSTIA

TABLE 3. Reanalyses used in this study. The grid spacing is given at 50°N for MERRA (square root of gridbox area and zonal × meridional spacing in parentheses).

Reanalysis	Resolution	Grid spacing (km)	Period	SST forcing	Reference
ERA-40	T159	126	1958–2001	HadISST1 (Rayner et al. 2003; Reynolds et al. 2002)	Uppala et al. (2005)
ERA-Interim	T255	79	1979 to present	(Several; see references)	Dee et al. (2011)
MERRA	2/3° × 1/2°	51 (48 × 56)	1979 to present	Reynolds et al. (2002)	Rienecker et al. (2011)

the blocking index used by Tibaldi and Molteni (1990) to a two-dimensional map of blocking frequencies at every grid point. In the AGP index, three conditions need to be fulfilled for a point at latitude ϕ_0 to be identified as blocked. The first condition is a reversal of the climatological equator–pole gradient of the 500-hPa geopotential height Z to the south of ϕ_0 :

$$\frac{Z(\phi_0) - Z(\phi_s)}{\phi_0 - \phi_s} > 0, \quad (1)$$

where ϕ_s is 15° south of ϕ_0 . The second condition requires westerly flow to the north of ϕ_0 :

$$\frac{Z(\phi_N) - Z(\phi_0)}{\phi_N - \phi_0} < -10 \text{ m (° latitude)}^{-1} \quad (2)$$

where ϕ_N is 15° north of ϕ_0 . The third condition is that the point is only considered blocked if the first two conditions are met for five consecutive days or more. As described by Scherrer et al. (2006), this persistence criterion is stricter than in some other studies (e.g., D’Andrea et al. 1998; Doblas-Reyes et al. 2001) so that the AGP typically captures mature blocking states and AGP blocking frequencies are comparatively low. We apply the blocking index to daily instantaneous 1200 UTC geopotential height fields from models and reanalyses for all Northern Hemisphere grid points between 35° and 75°N. All model and reanalysis fields are regridded to a common $1.875^\circ \times 1.25^\circ$ grid before the blocking identification is applied.

The AGP blocking index we use is a common (Scherrer et al. 2006; Anstey et al. 2013; Berckmans et al. 2013) albeit to some extent subjective choice, and other indices have been suggested in the literature [see, e.g., Barriopedro et al. (2010) for an overview]. An intercomparison of blocking identification methodologies is outside the scope of this study, but we recognize that the existence of different blocking indices may make it more difficult to directly compare between different studies. We refer to Scherrer et al. (2006) for a comparison of the AGP index with two other blocking indices. Additionally, the supplemental material shows examples of composites illustrating how blocking is captured with

the AGP index for different seasons and locations and what the associated anomalies in surface pressure, temperature, and precipitation are.

3. Blocking in reanalyses

In this preliminary section, we show how blocking is represented by the different reanalyses that serve as the reference for the model simulations evaluated in section 4. Figure 1 shows the climatological blocking frequency from ERA-40 and ERA-Interim for the four seasons. During winter (Fig. 1a), we reproduce the well-known (e.g., Anstey et al. 2013) distribution with blocking predominantly occurring in the Atlantic–European and Pacific sectors. Within the Atlantic–European sector, preferred regions of blocking occurrence are over southeast Greenland, the North Sea, and the Ural Mountains. In spring (Fig. 1b), two maxima of blocking frequency over Europe can be seen to the west and north of the British Isles and to the east of the Baltic Sea. In summer, blocking events are identified over a wide range of longitudes spanning Greenland, Eurasia, and Alaska, and there is no clear distinction between a region of Atlantic and Pacific blocking. Finally, during autumn, the spatial distribution of blocking occurrence is similar to that in spring, but the frequency is smaller than in spring throughout the Northern Hemisphere.

We use Fig. 1 to introduce some regions, outlined by the blue boxes, which will be used to calculate area-averaged blocking statistics presented later in the paper. We refer to these regions as Greenland (GL), Atlantic (ATL), Baltic (BAL), and Pacific (PAC). We also consider a northern Europe (NEU) area, which is the joint area of ATL and BAL and better corresponds to the climatological spatial distribution of blocking frequency during winter.

Time series of the interannual variability of blocking frequency are shown in Fig. 2. It can be seen that there is very close agreement between the ERA-40, ERA-Interim, and MERRA products in Europe (Figs. 2a,b) and also close agreement in the PAC and GL regions (Figs. 2c,d) where fewer in situ observations are assimilated by the reanalyses. This close agreement is not surprising since blocking anticyclones are slow-moving synoptic-scale systems that should be captured by all

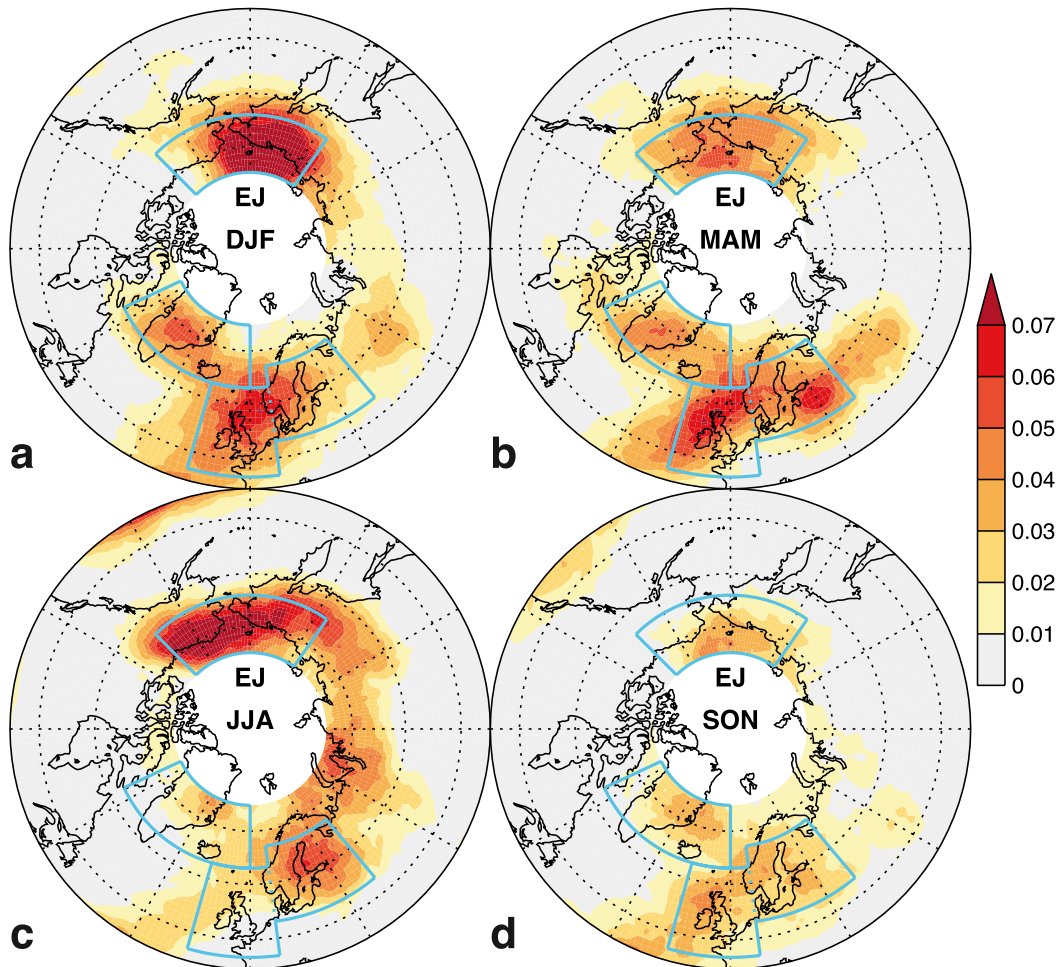


FIG. 1. Climatological-mean reanalysis blocking frequency (fraction of blocked days) based on concatenating ERA-40 (1962–78) and ERA-Interim (1979–2011) for (a) December–February, (b) March–May, (c) June–August, and (d) September–November. The light blue lines show five regions: ATL (47°–63°N, 16°W–7.5°E), BAL (53°–67°N, 7.5°–40°E), PAC (64°–75°N, 145°–225°E), GL (63°–75°N, 295°E–0°), and NEU, which is the joint area of ATL and BAL.

of the reanalyses. This agreement also justifies using a concatenated dataset from two reanalyses (Fig. 1) as the reference against which model simulations are evaluated.

Also evident from Fig. 2 is the large variability of blocking frequency at interannual and possibly longer time scales. This large internal variability needs to be accounted for in the identification of model biases. For the examples shown in Fig. 2, the coefficient of variation of the time series takes values between about 0.5 and 1. A rough estimate of the minimal time series length n necessary to identify a statistically significant difference in the mean blocking frequency can be obtained under the simple assumptions of a z test. A brief calculation shows that then $n = (1.96 c_{\text{var}}/\beta)^2$, where $\beta = 1 - (\mu_1/\mu_2)$, $\mu_1 \leq \mu_2$, is the relative difference between the two time series means μ_1 and μ_2 , c_{var} is the

coefficient of variation of time series 2, and 1.96 is the quantile of the standard Gaussian corresponding to the customary confidence level of 95%. Taking $\beta = 0.2$ (i.e., an underestimation of the mean blocking frequency by 20%) yields $n = 24$ yr for $c_{\text{var}} = 0.5$ and $n = 96$ yr for $c_{\text{var}} = 1$. These estimates show that the model ensemble used here (Table 2) is suitable for identifying any large biases with respect to the 50-yr reanalysis climatology shown in Fig. 1, as well as large sensitivities to model resolution.

4. Resolution sensitivity

a. Winter

Figures 3b–k show the blocking frequency for the different models and resolutions in winter. The reference reanalysis field already shown in Fig. 1a is repeated here

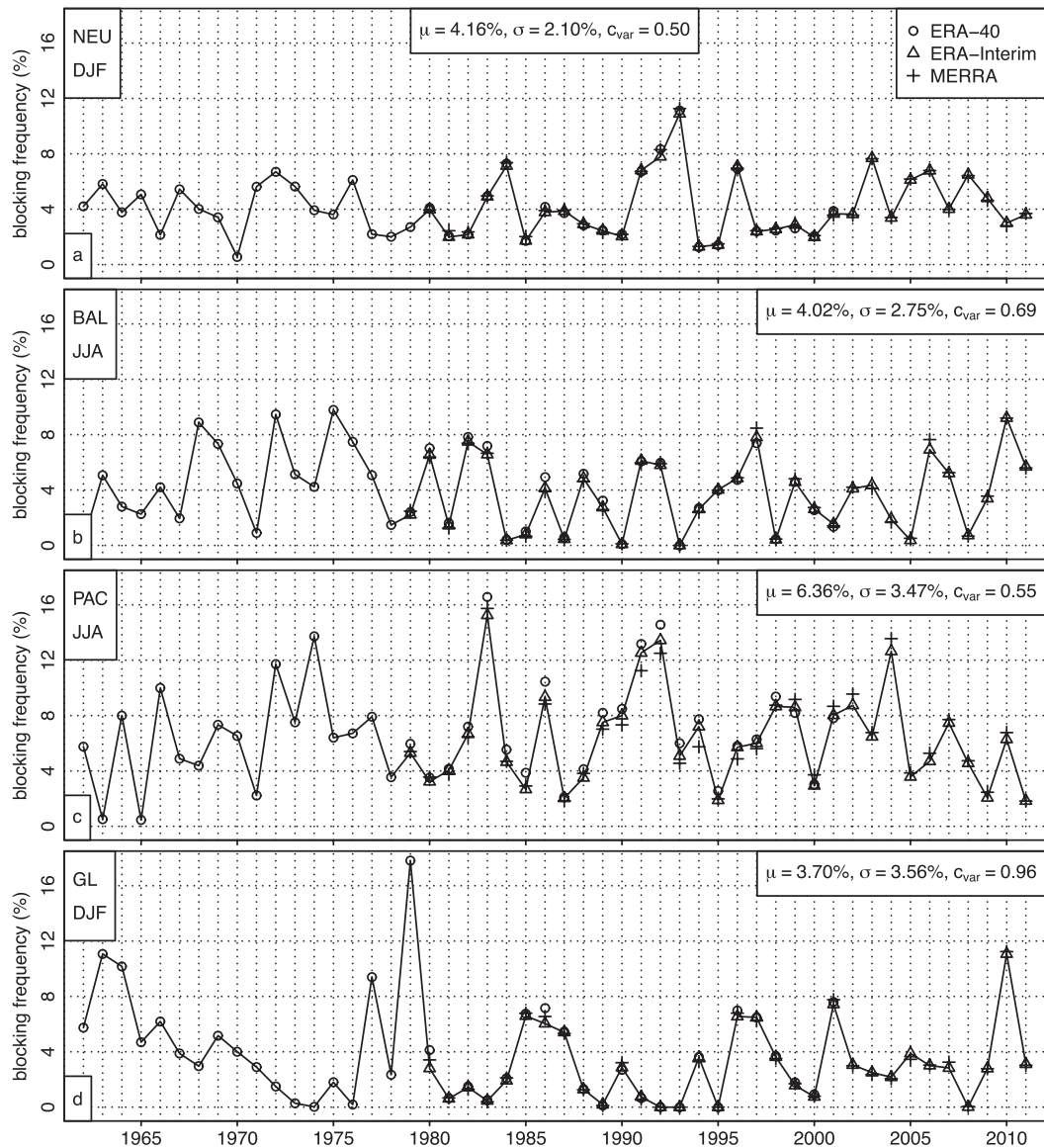


FIG. 2. Examples of 50-yr time series of blocking frequency spatially averaged over the regions shown in Fig. 1 for boreal winter or summer. Symbols show, ERA-40 (circles; 1962–2001), ERA-Interim (triangles; 1979–2011), and MERRA (plus signs; 1979–2011). The solid line shows the concatenated reference time series composed of ERA-40 (1962–78) and ERA-Interim (1979–2011). The inset shows the mean μ , standard deviation σ , and coefficient of variation c_{var} of this reference time series.

for convenience in Fig. 3a. All models represent the hemispheric-scale pattern of blocking frequency maxima in the Atlantic–European and Pacific sectors, yet they exhibit biases in the details of the spatial distribution and tend to underestimate the blocking frequency at all resolutions. Two regions of high blocking frequency over Greenland and in the region of the Ural Mountains are captured by all of the models. In contrast, the low-resolution models (Figs. 3b,d,g,j) underestimate the blocking frequency over the North Sea and show

comparatively high blocking frequency over the south of the British Isles and the Celtic Sea instead. This bias is reduced in the high-resolution models (Figs. 3c,f,i,k). The winter domain-mean blocking frequencies are shown in Fig. 4. The main result of Fig. 4 is that three out of the four models (CAM5, IFS, and UM) strongly underestimate the winter blocking frequency. There is a slight improvement with resolution in the NEU domain for CAM5 and IFS, yet considerable negative biases remain for most of the high-resolution models: the NEU

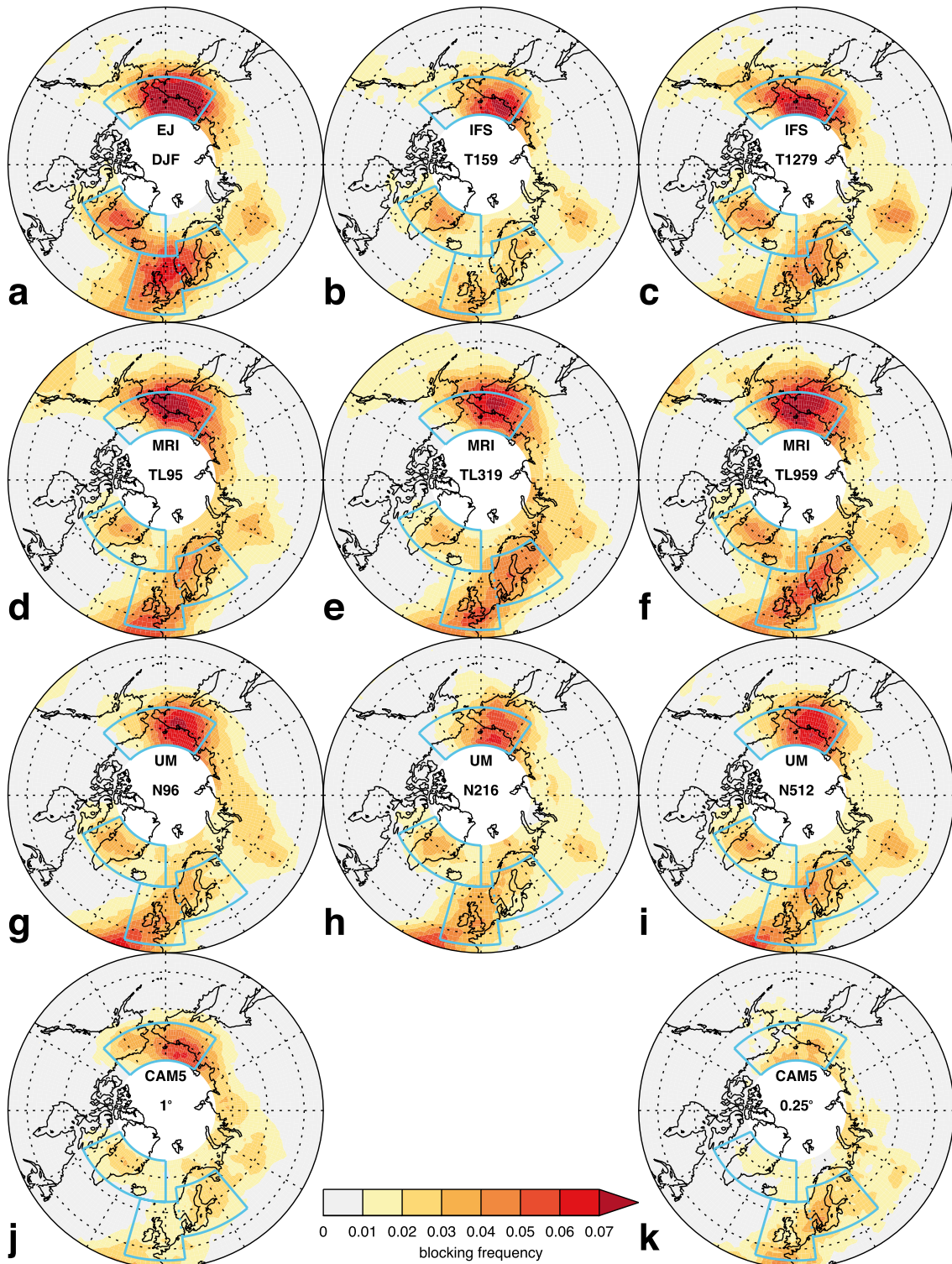


FIG. 3. December–February climatological and ensemble-mean blocking frequency (fraction of blocked days). (a) ECMWF reanalyses as in Fig. 1 and at resolutions for (b) IFS at T159, (c) IFS at T1279, (d) MRI at TL95, (e) MRI at T319, (f) MRI at T959, (g) UM at N96, (h) UM at N216, (i) UM at N512, (j) CAM5 at $1.3^\circ \times 0.9^\circ$, and (k) CAM5 at $0.31^\circ \times 0.23^\circ$.

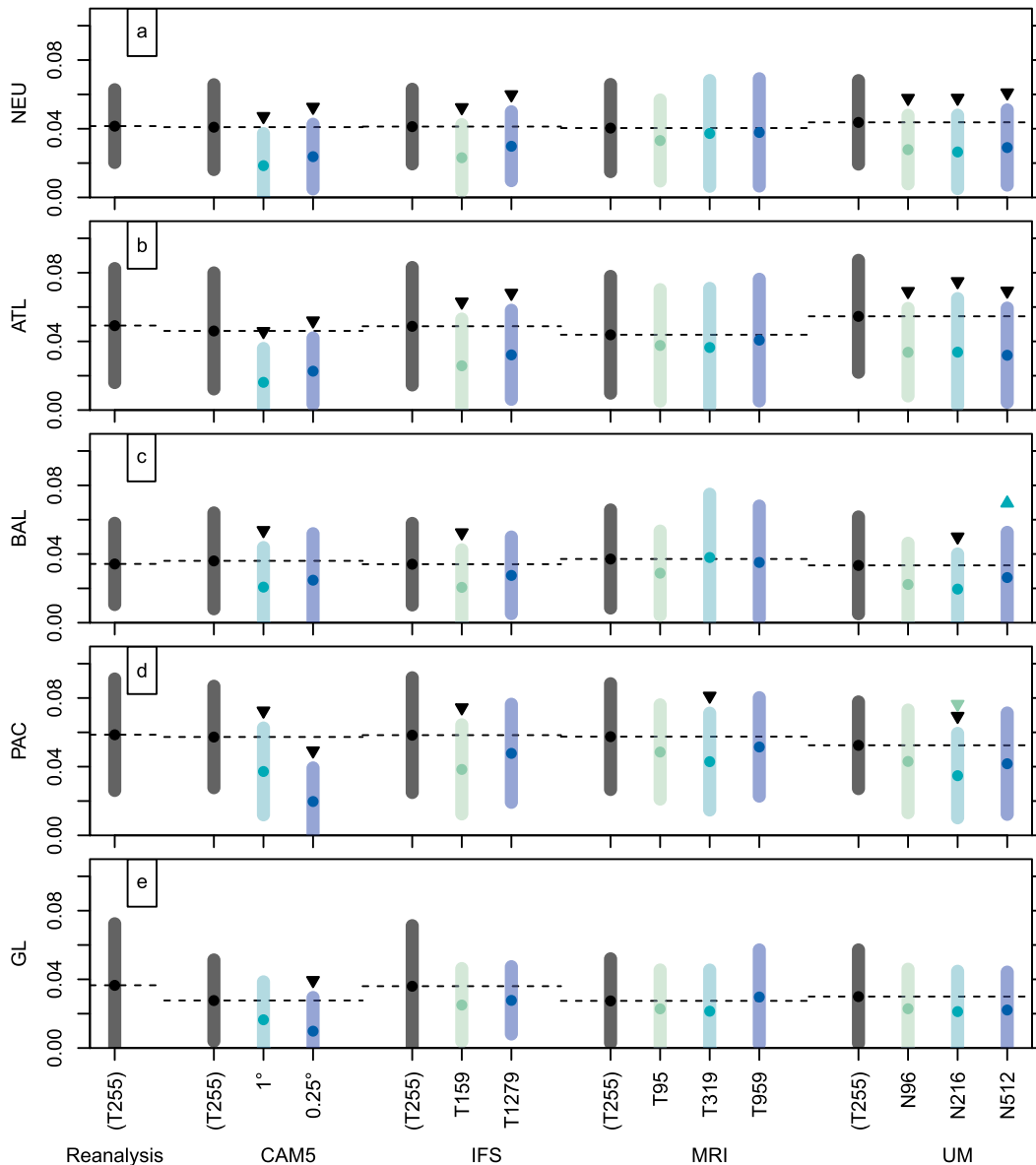


FIG. 4. December–February climatological and ensemble-mean blocking frequency for regions defined in Fig. 1. ERA-40–ERA-Interim values (as in Fig. 1) are shown for 1962–2011 on the left axis in terms of the mean (black dot and horizontal dashed line) plus/minus the ensemble mean of one standard deviation of interannual variability (gray bar). Reanalysis blocking frequencies are also shown for each of the simulation periods of the four models. Colored green-blue dots and bars show the same information for the four models at different resolutions. Triangles indicate significant test results for differences; for example, the downward triangles in (a) for CAM5 at 1° and 0.25° resolution indicate that the blocking frequency in these two models is significantly smaller than in the reanalysis. In the same way, colored triangles show significant differences between different resolutions of a model. The test employed is a *t* test comparing the mean of two samples composed of the yearly ensemble-mean blocking frequencies of the two datasets at hand.

underestimation is 43% for CAM5, 28% for IFS, 9% for MRI, and 30% for the UM.

b. Spring

Figures 5 and 6 show that the resolution sensitivity is larger in spring (March–May) than in winter. This is seen

robustly across the ensemble; comparing the low-resolution results (Figs. 5b,d,g,j) with the high-resolution results (Figs. 5c,f,i,k) in the Euro-Atlantic sector shows an increase in simulated blocking and a reduction of the bias with resolution. The domain-mean values shown in Fig. 6 confirm that this increase is

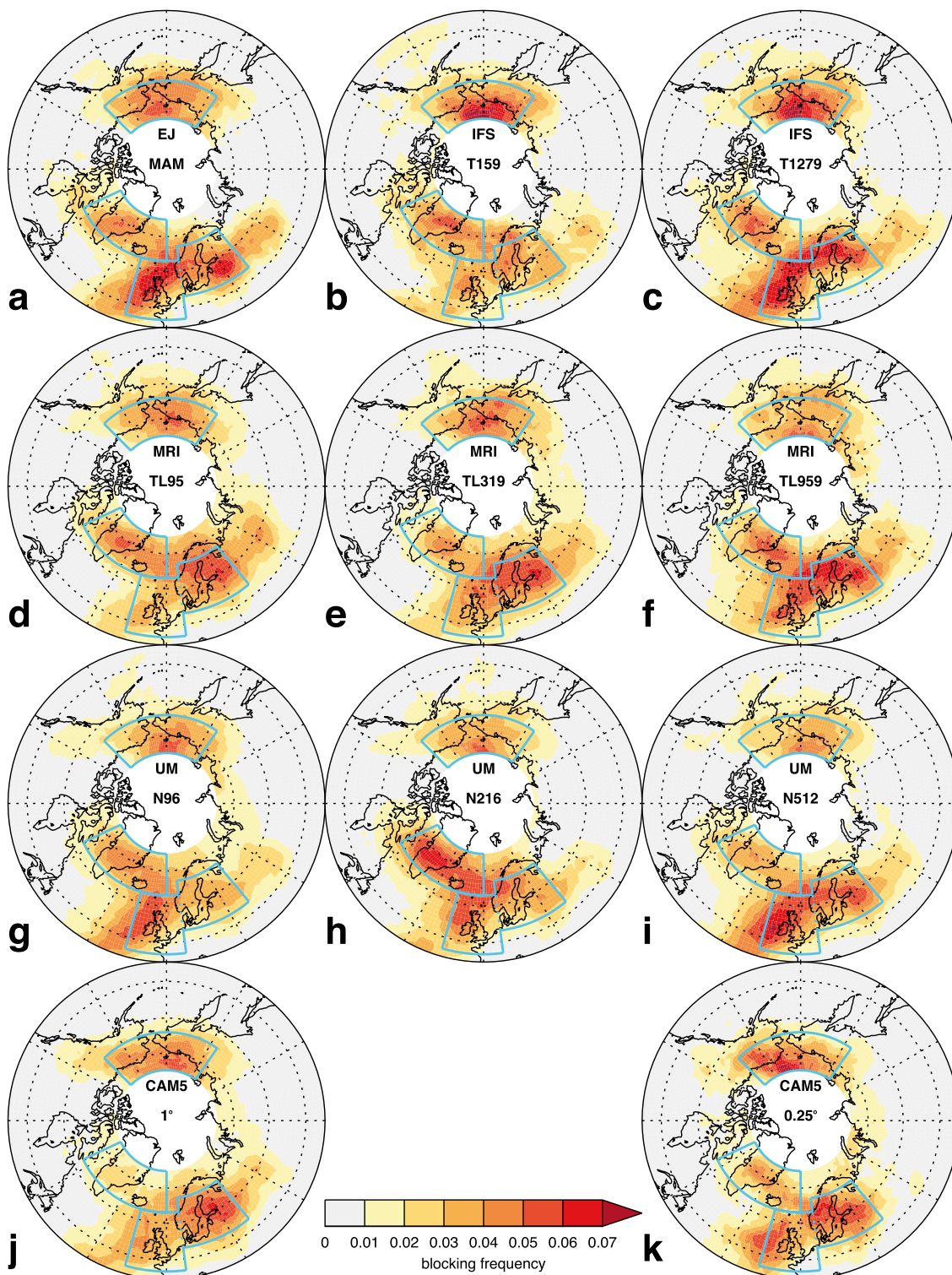


FIG. 5. As in Fig. 3, but for spring (March–May).

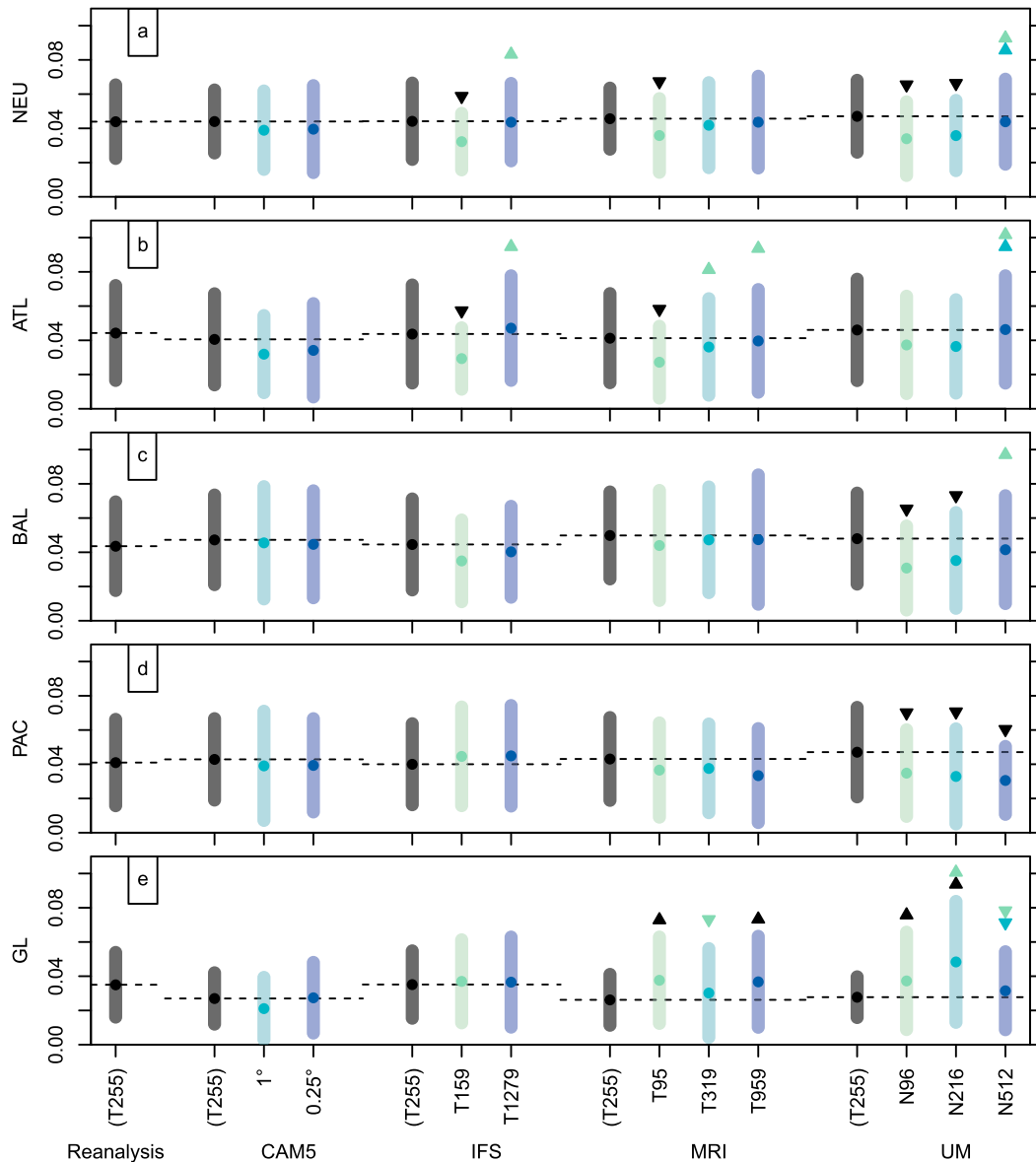


FIG. 6. As in Fig. 4, but for spring (March–May).

significant in three models (IFS, MRI, and UM) in the NEU domain. The spatial pattern of blocking frequency also agrees better with the reanalyses in the high-resolution models. In the Euro-Atlantic sector, two distinct regions of high blocking frequency (i) over Greenland and (ii) over an arc-shaped region stretching from west of Scotland to east of the Baltic Sea are more markedly represented in the higher-resolution models. Pacific blocking is captured fairly well overall and at all resolutions but underestimated by about 20% in the UM. Figures 5 and 6 also show that, while there are clear limitations in how the models represent blocking during the spring, the domain-mean biases are smaller

than during winter. This is also seen in the low-resolution models.

c. Summer

During summer (June–August; Fig. 7), there is no systematic sensitivity in the model biases to resolution both in the Euro-Atlantic and Pacific sectors. The pattern of the biases differs somewhat between the models, however. In the IFS, the blocking frequency is underestimated nearly everywhere and blocking is restricted to too-high latitudes. In the MRI model, the geographical distribution of blocking is in fairly close agreement with the reanalyses, but the blocking frequency is underestimated in the PAC region. In the UM,

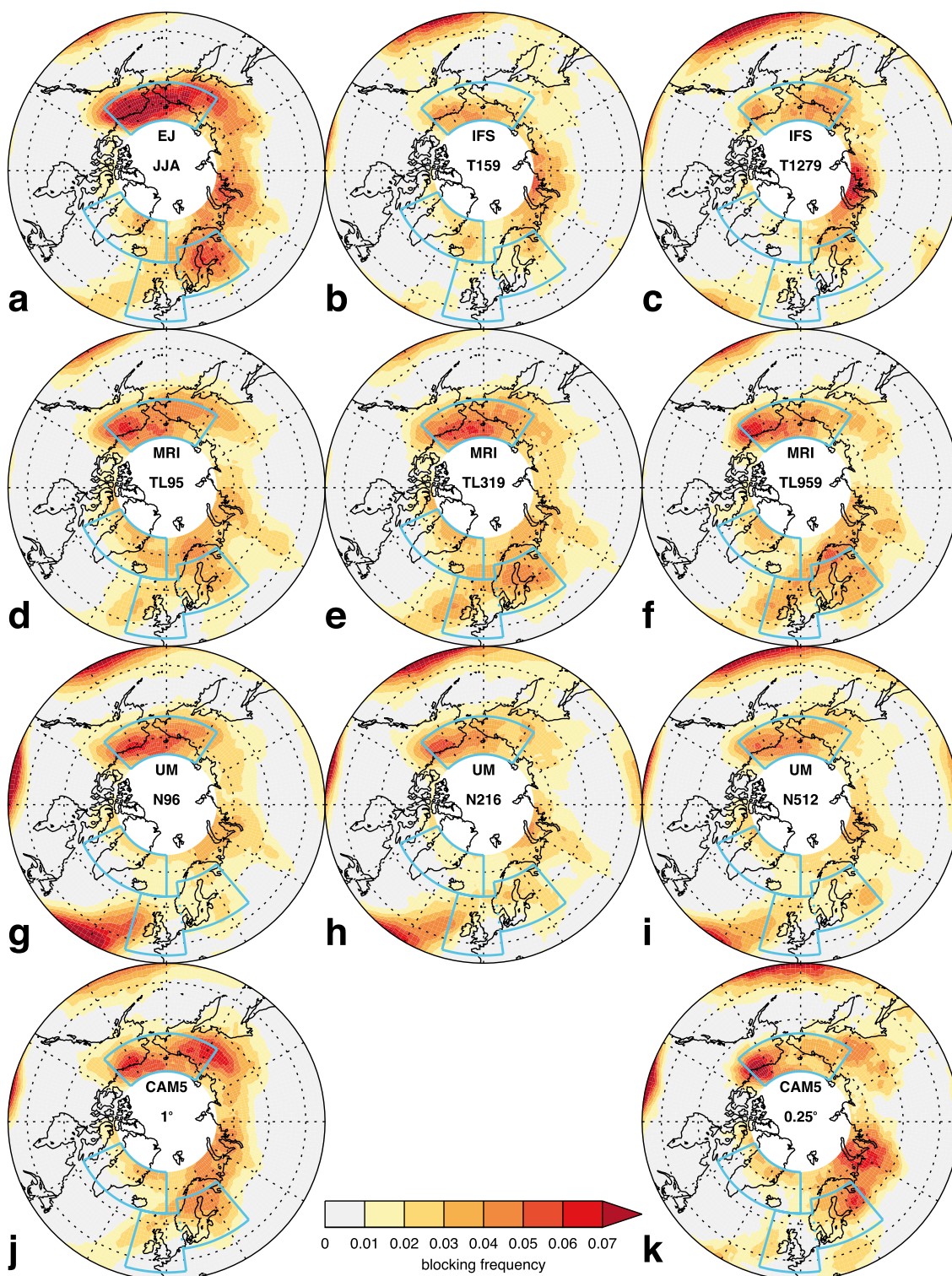


FIG. 7. As in Fig. 3, but for summer (June–August).

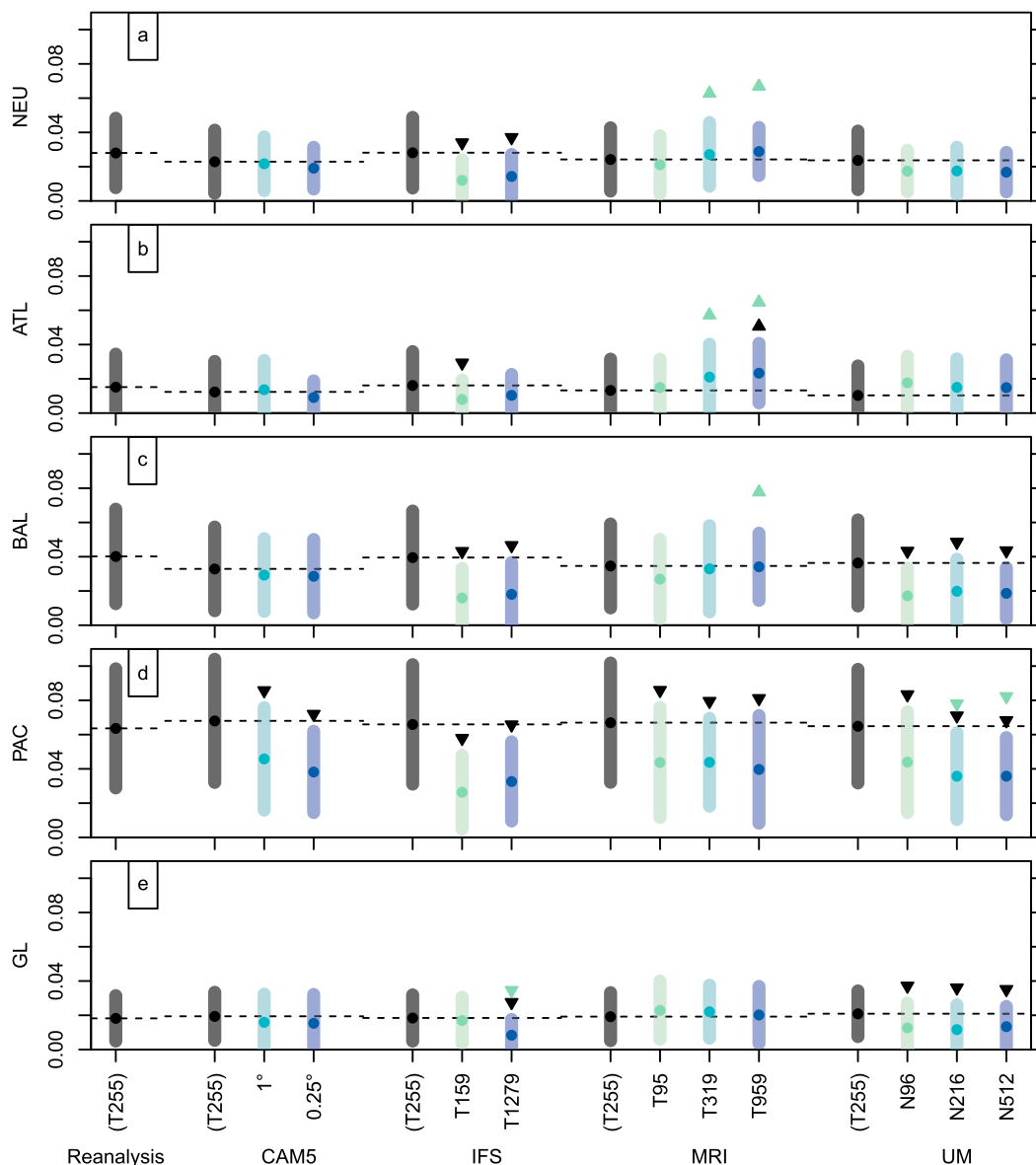


FIG. 8. As in Fig. 4, but for summer (June–August).

the spatial distribution agrees closely with the reanalysis blocking, but the blocking frequency is underestimated throughout the Northern Hemisphere. There is close agreement between the CAM5 blocking frequency pattern and the reanalyses, and small-scale differences especially between the high-resolution CAM5 (Fig. 7k) and the reanalyses may be due to sampling variability for this single simulation. The domain-mean blocking frequencies are shown in Fig. 8. The two regions with high reanalysis summer blocking frequency are PAC and BAL. In the PAC region, blocking is considerably underestimated by all four models, by between 58% (IFS at

T159) and 28% (CAM5 at 1°). The IFS and UM also significantly underestimate blocking in the BAL region, both by approximately 50%, whereas CAM5 and MRI agree fairly closely with the reanalysis in BAL.

d. Autumn

Finally, during autumn (September–November; Figs. 9 and 10), the blocking frequency biases are comparatively small for all resolutions and models, and accordingly the domain-mean biases and resolution sensitivity are not significant for many of the regions–models. The most apparent bias is the underestimation of PAC

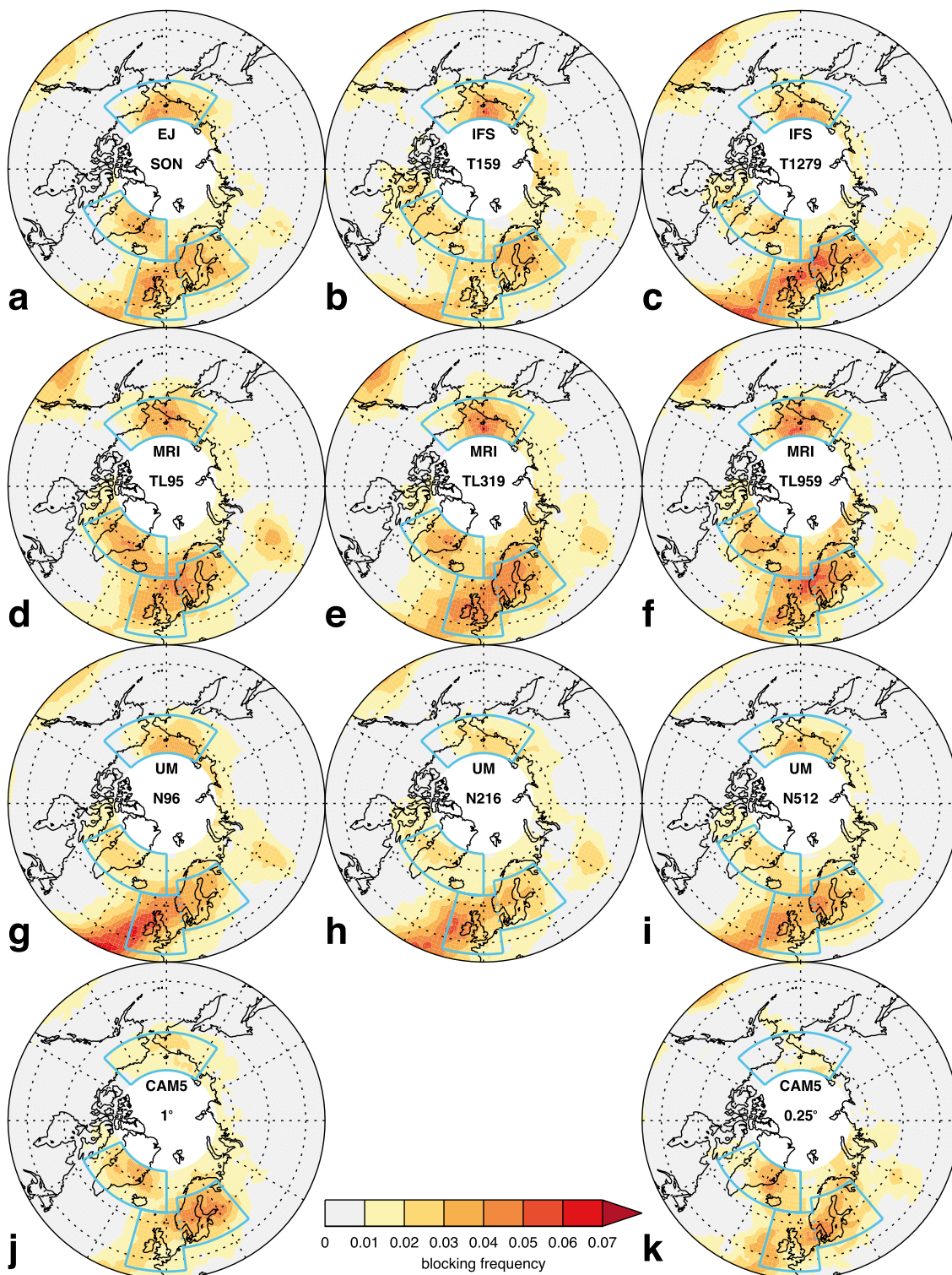


FIG. 9. As in Fig. 3, but for autumn (September–November).

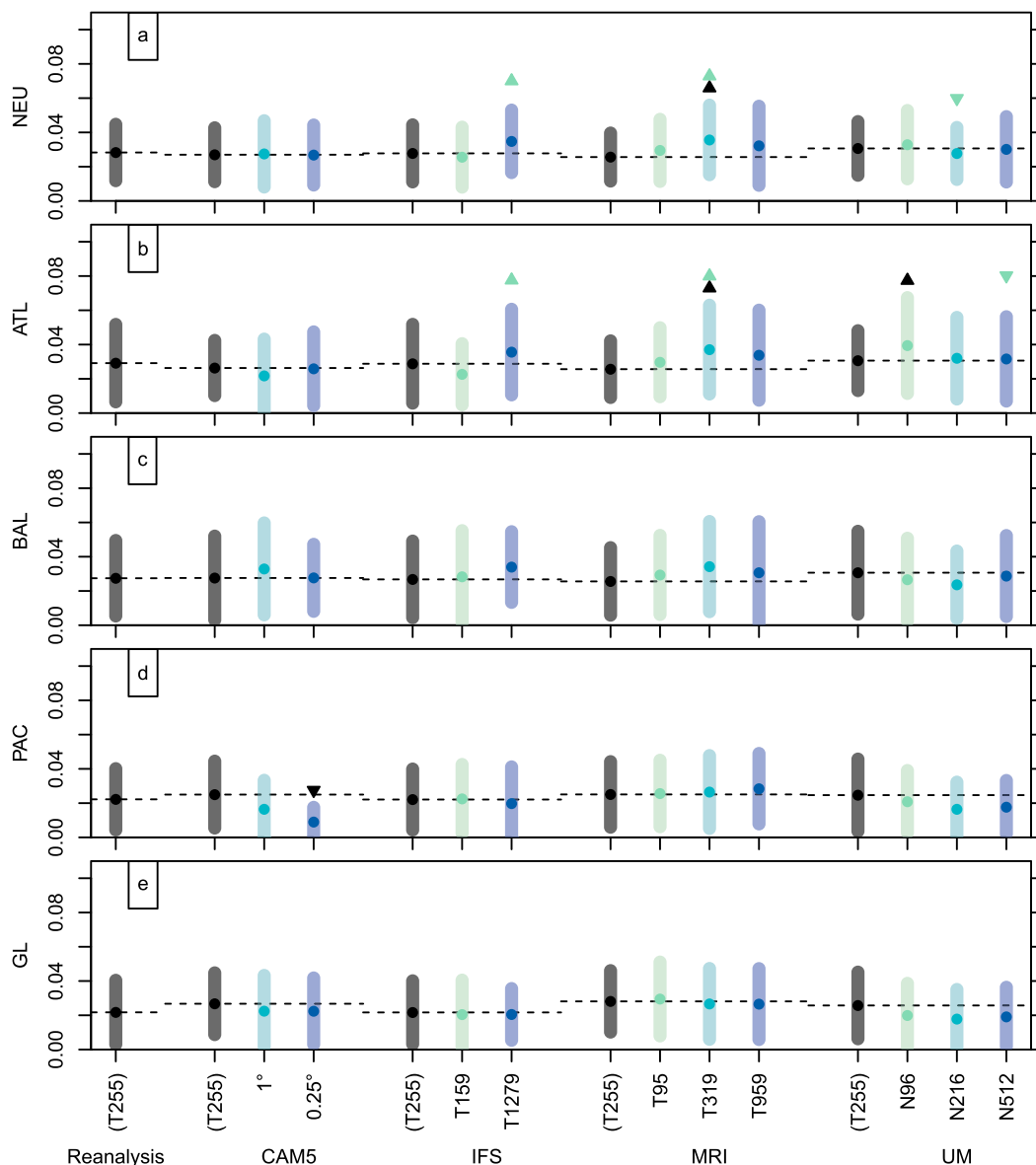


FIG. 10. As in Fig. 4, but for autumn (September–November).

blocking in the CAM5 at 2° resolution (Figs. 11k and 12d) by about 60%.

e. Pattern correspondence

A quantitative assessment of the overall correspondence of the simulated and reanalysis blocking frequency patterns in the Atlantic–European sector is provided in Fig. 11. Figure 11 shows scatterplots of the root-mean-square error (RMSE) and the spatial correlation of the model-simulated blocking frequency pattern with the reanalysis pattern shown in Fig. 1. As the interannual variability is better sampled in the ensemble-mean blocking frequency pattern, the pertaining values of the

RMSE (the spatial correlation) tend to be smaller (larger) than for individual ensemble members. This fact needs to be considered for models where the ensemble size differs at the different resolutions (Table 2).

The scatterplots in Fig. 11 confirm and in some cases show more clearly if there is a significant improvement in the representation of Atlantic blocking with resolution. For example, for the UM (Fig. 11d) an improvement with resolution is seen in the ensemble mean for all four seasons, yet only during spring and summer this improvement is large compared with the typical difference between ensemble members as

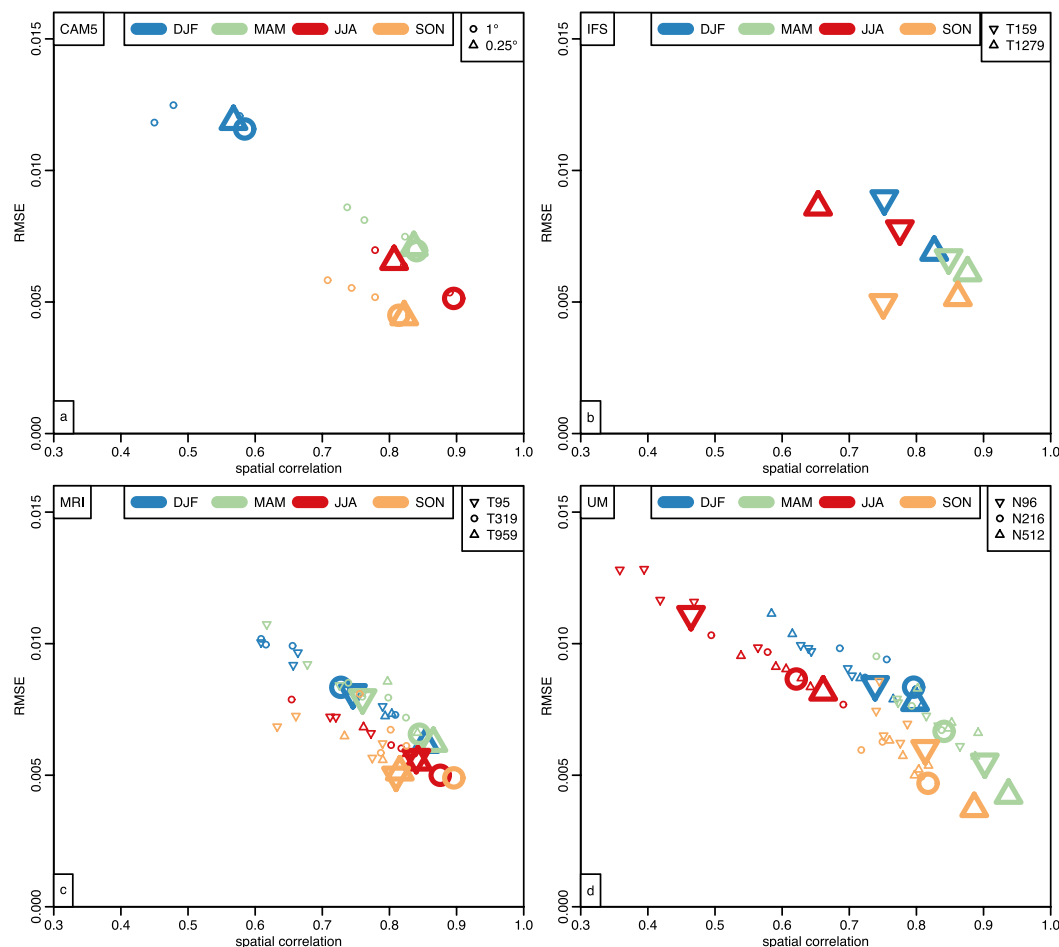


FIG. 11. Blocking frequency root-mean-square error and spatial correlation with respect to the reanalysis blocking frequency field shown in Fig. 1 for the Atlantic–European sector (45° – 75° N, 280° – 80° E). (a)–(d) The four different models; small symbols correspond to ensemble members and large-thickened symbols to the ensemble mean (see Table 2): N96 (upside down triangles), N216 (circles), and N512 (triangles); and DJF (blue), MAM (green), JJA (red), and SON (orange).

shown by the fairly good separation of the “clouds” of points corresponding to the low- and high-resolution ensembles. This separation provides a qualitative evaluation of the statistical significance of the differences in RMSE and correlation coefficient between simulations at different resolutions. While all models show an improved representation of blocking during spring, as was also shown in Fig. 5, they do not necessarily agree on improvements in other seasons. For example, while there is a clear improvement during summer for the UM, the MRI and IFS show improved Atlantic blocking in winter and little change or even a deterioration during summer. Despite the biases remaining in the high-resolution models, Fig. 11 shows an overall improvement in the representation of blocking in the Atlantic sector with higher resolution. Additionally, Fig. 11 also illustrates how a sufficient

number of models–ensemble members are needed in order to assess the sensitivity to resolution unequivocally.

Analogous scatterplots for the Pacific sector (not shown) do not reveal any systematic sensitivity to resolution. This is consistent with results showing that the simulation of Pacific blocking is not sensitive to horizontal resolution, for example in the CMIP5 ensemble (Anstey et al. 2013) and in MRI-AGCM3.1 (Matsueda et al. 2009). The sensitivity to resolution seen here for the European region in winter, and possibly in spring, is also consistent with the findings that for CMIP5 models (i) European blocking and storm-track biases are closely associated (Zappa et al. 2014) and (ii) winter storm-track biases in the North Atlantic are reduced at higher resolution (Zappa et al. 2013).

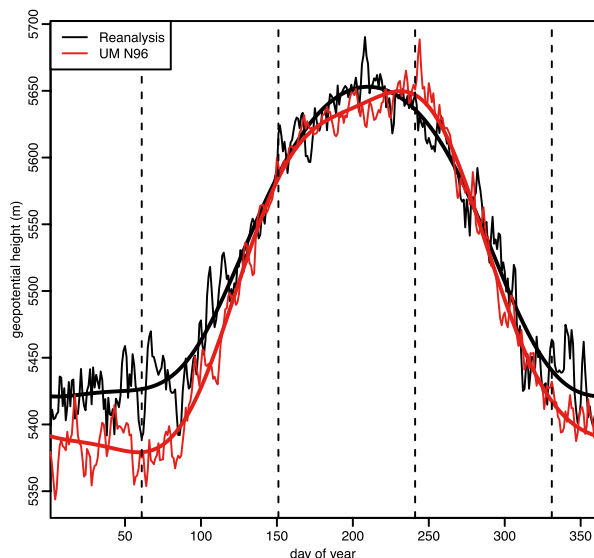


FIG. 12. Illustration of bias correction of the 500-hPa geopotential height field (m) for a single grid box at 56.25°N , 0° and for the UM at N96 resolution (red) with respect to ERA-40–ERA-Interim data as in Fig. 1 (black). Thin lines show the daily climatological-mean value, and thick lines show the daily climatological-mean value after low-pass filtering with a cutoff frequency at $(90 \text{ days})^{-1}$. Vertical dashed lines show the canonical Northern Hemisphere seasons.

5. Blocking and mean-state biases

In this section, we follow the approach of Scaife et al. (2010) to determine the degree to which the blocking biases in the models are associated with their mean-state biases. We apply a correction to the mean of each model 500-hPa geopotential height output and then recalculate the blocking index based on the bias-corrected height field. The procedure is illustrated in Fig. 12 for a single model and grid point: the thin red line shows the daily climatological-mean geopotential height for the UM at N96 resolution at this grid point. The thick red line is obtained by low-pass filtering this data with a cutoff frequency at $(90 \text{ days})^{-1}$. The thick black line shows the same daily low-pass-filtered climatology for the reanalysis data, and the difference between the two thick lines defines the model “mean” bias on each day. Repeating this at each grid point defines the model bias at each grid point and for each day of the year, and the model geopotential height is now corrected for this bias before calculating the blocking climatology.

Figures 13b,e,h,k show the winter blocking climatology obtained after correcting the mean geopotential height to reanalysis in the lowest-resolution version of the four models. This can be compared with the uncorrected blocking frequency and the reference reanalysis climatology shown in Fig. 3. It can be seen that

the bias correction yields higher blocking frequencies over north and west Europe in better agreement with the reanalysis (Fig. 3a) than the uncorrected low-resolution models (Figs. 3b,d,g,j). There is some consistency between the winter mean geopotential height bias of the four low-resolution models (shown in Figs. 13a,d,g,j) and the effect of bias correction on the blocking climatology. All models have a low height bias over northwest Europe consistent with the general increase in blocking frequency upon bias correction. For the MRI model whose height bias over northwest Europe is fairly small, the effect of bias correction is fairly small as well.

However, similar to the uncorrected climatologies, the bias-corrected climatologies misplace the North Sea maximum of blocking occurrence southwestward over the south of the British Isles and the Celtic Sea. This shows that the mean-state bias, defined as described above, can only partly account for the blocking biases seen in the low-resolution models.

We also show the resolution sensitivity in the winter mean 500-hPa geopotential height for the four models in Figs. 13c,f,i,l. Over the Atlantic and Eurasia, the increase in resolution largely reduces the biases in the low-resolution models. This is consistent with the slight enhancement in Euro-Atlantic blocking seen with resolution. Again, the resolution sensitivity of the mean geopotential height cannot fully explain the change in the blocking climatology with resolution. For example, both the IFS and MRI models simulate higher occurrence of blocking over the North Sea at higher resolution, while the geopotential height field in this area changes strongly with resolution in the IFS model, but not so in the MRI model.

For spring (Fig. 14), we find that the blocking climatologies based on bias-corrected height data agree overall better with the reanalyses (Fig. 5a) than the uncorrected climatologies of the low-resolution models (Figs. 5b,d,g,j). As in winter, however, the association between mean-state and blocking biases is far from perfect and varies strongly between the models; in the low-resolution UM, for example, there is a pronounced negative height bias over central–northern Europe (Fig. 14g), and correcting for this height bias yields a strongly improved blocking climatology and higher blocking frequency in the NEU area (Fig. 14h). Also, at high resolution this negative height bias is smaller than at low resolution (Fig. 14i), which is consistent with the improvement in the simulated blocking seen with resolution (Figs. 5g,h,i). In the low-resolution IFS, there is a negative height bias in the North Atlantic–European midlatitudes and a positive bias in the Arctic, particularly in the region of the Baffin Bay (Fig. 14a).

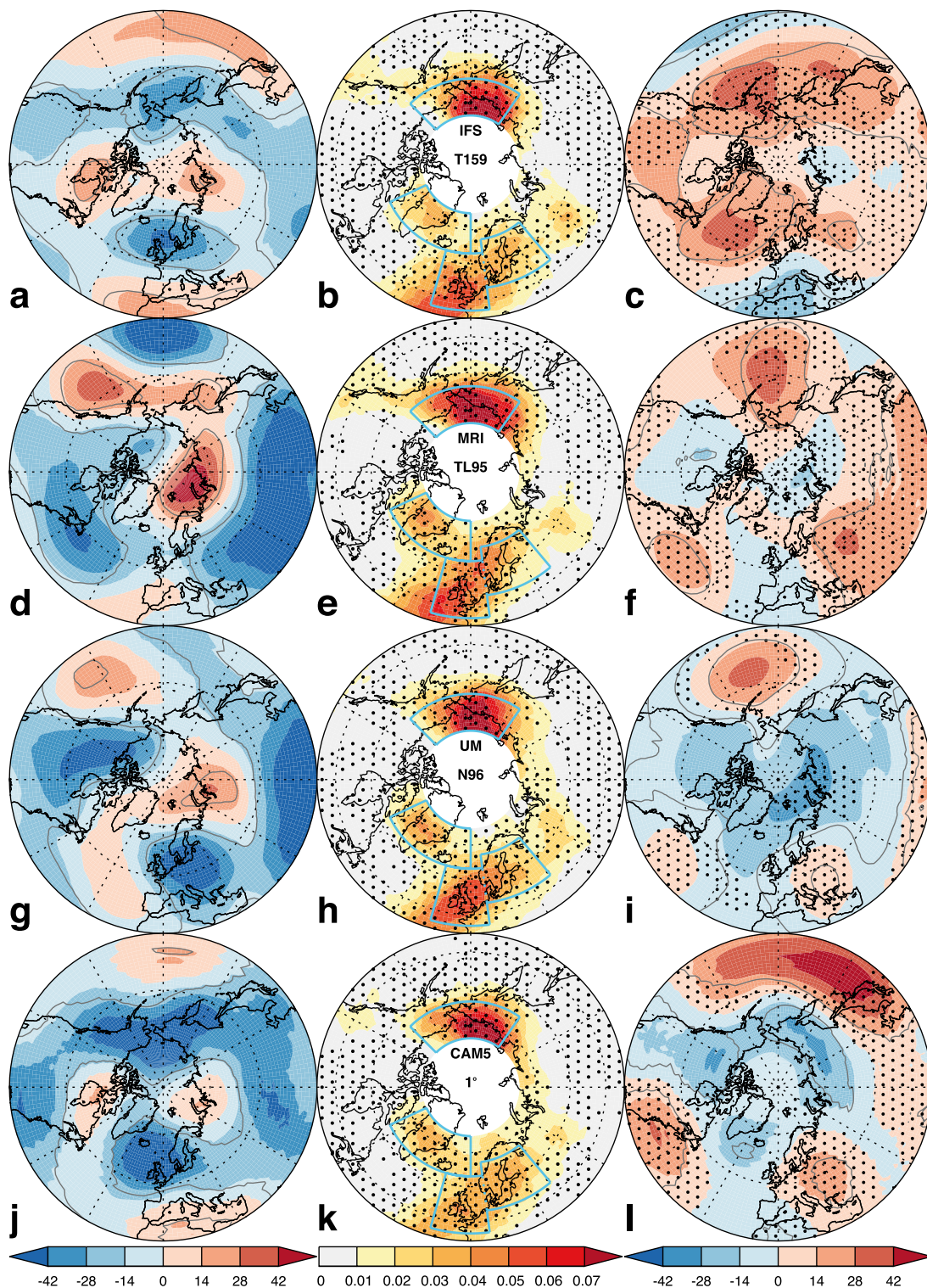


FIG. 13. December–February (left) 500-hPa geopotential height bias (m), (center) blocking frequency calculated from bias-corrected geopotential height data for lowest-resolution model (e.g., N96 for the UM), and (right) 500-hPa geopotential height difference (m) for the highest minus lowest-resolution model (e.g., N512 – N96 for the UM). The models are (a)–(c) IFS, (d)–(f) MRI, (g)–(i) UM, and (j)–(l) CAM5. Gray lines enclose areas of statistically significant geopotential height differences. Stippling shows regions where correcting the height bias reduces the blocking bias, as in (b),(e),(h),(k); and where the height bias decreases with the resolution increase, as in (c),(f),(i),(l).

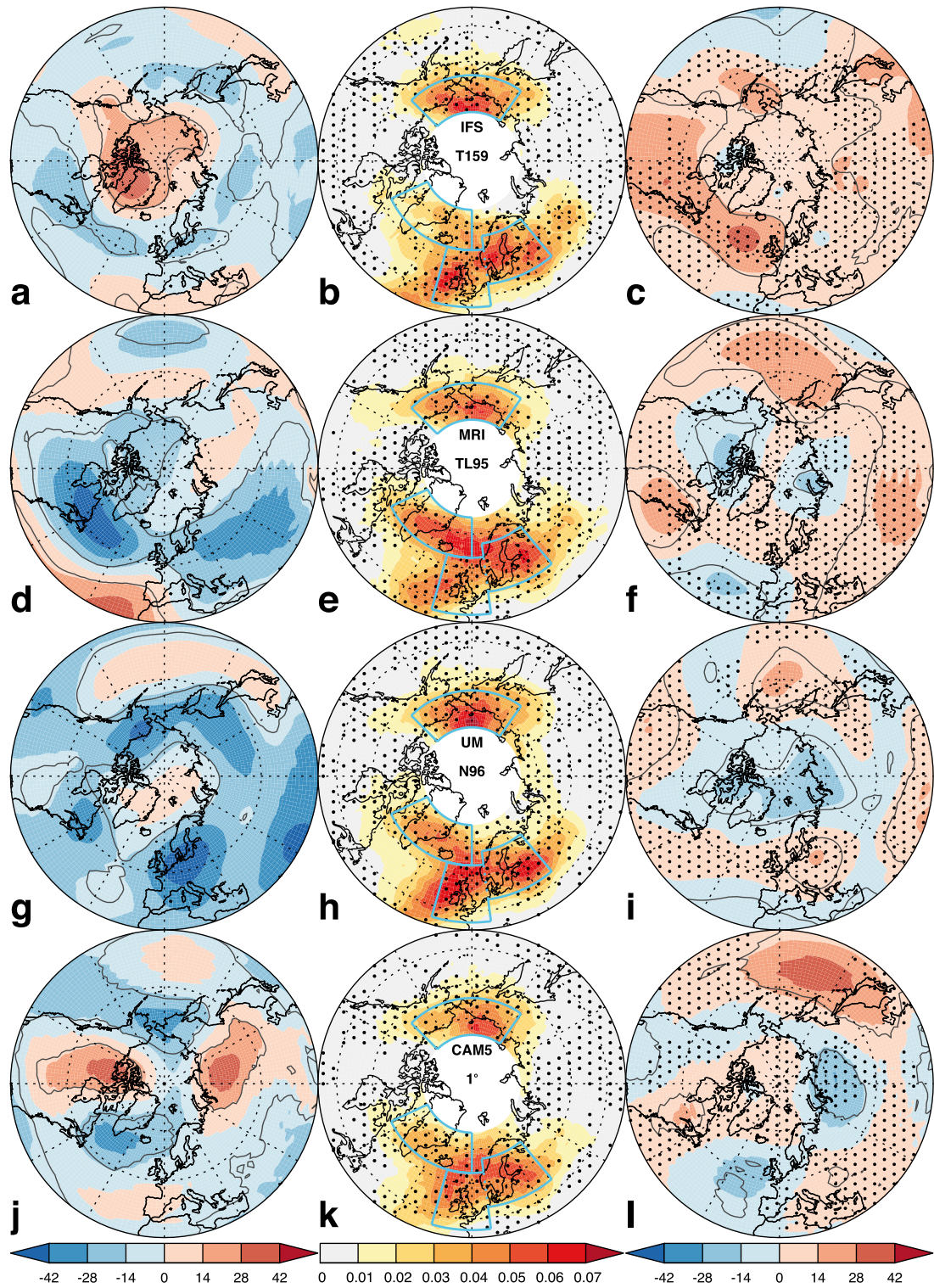


FIG. 14. As in Fig. 13, but for spring (March–May).

Correcting for this bias has the expected mixed effect on the blocking climatology, namely more frequent NEU blocking in better agreement with the reanalyses and less frequent GL blocking in worse agreement with the reanalyses (Fig. 14b and Figs. 5a,b). Also the change in the geopotential height bias with resolution (Fig. 14c) is significant over the ATL area and very small over the BAL area, while the improvement in the simulated blocking (Fig. 5c) can be seen in both areas and does not seem to be closely associated with the mean-state bias.

In the summer, the low-resolution blocking biases appear to be more closely associated with the mean-state biases than during winter and spring (Fig. 15 and Fig. 7); for example, all four models have a positive height bias over the Gulf of Alaska, whose correction yields more frequent PAC blocking, in better agreement with the reanalyses. Also, with the exception of CAM5, the models have a negative height bias in the BAL region and a positive bias over the Arctic, leading to more frequent and more realistic blocking frequency when corrected. As discussed previously, however, the improvement in the simulated blocking with higher resolution is fairly small. Even in the case of the MRI model, whose mean-state bias is considerably smaller at high resolution (Figs. 15d,f), there is only a slight improvement in the simulated blocking (Figs. 7d–f). Large biases remain at the high resolution, showing that the reduction of a mean-state bias does not always imply a similar reduction of the blocking bias.

As shown previously (Fig. 9), both the blocking biases and their resolution sensitivity are smaller in autumn than in the other seasons. Here, we find that the effect of bias correcting the geopotential height field also has a fairly small, but beneficial, effect on the blocking climatology (not shown). The height biases themselves and their resolution sensitivity, however, are of similar magnitude to those in the other seasons.

6. Conclusions

We have evaluated the representation of Northern Hemisphere blocking in an ensemble of four AGCMs whose atmospheric resolution is increased from more than 100- to about 25-km horizontal grid spacing. Simulations at this high resolution are still difficult and costly to carry out, and few such simulations of sufficient length are available. We have analyzed here, for the first time, a multimodel ensemble of such simulations and are therefore, for the first time, able to document how robust the resolution sensitivity of blocking is at this scale. Overall, there is a clear improvement in the simulated Euro-Atlantic blocking with resolution. At the same

time, considerable blocking frequency biases remain in the high-resolution models. For example, three of the four high-resolution models (CAM5, IFS, and UM) continue to underestimate European winter blocking frequency by about one-third, and two models (IFS and UM) underestimate summer blocking frequency in the Baltic area by about 50%.

The degree to which simulated Euro-Atlantic blocking improves with resolution depends on the season and in some cases on the particular model. The clearest improvement is seen in spring, and it is robust across the ensemble, eliminating most of the bias. Smaller improvements, which are also robust across the ensemble, are seen in winter and autumn, whereby it should be noted that the biases in autumn are smaller than those in the other seasons for all models, even at the low resolutions. In summer, the resolution sensitivity is small and a significant improvement is only found for the UM. In the Pacific, we do not find a systematic sensitivity to resolution, except for CAM5 where there is some deterioration with increasing resolution in all seasons.

We have investigated the relationship between mean-state and blocking biases. This has been done by correcting the model mean geopotential height field to the corresponding reanalysis value while retaining the model geopotential height variability and then recalculating the blocking climatology. This separation is approximate because of the interaction between the mean state and eddies but can still provide a qualitative idea of how closely mean-state and blocking biases are associated with one another (Scaife et al. 2010). In agreement with previous studies (Scaife et al. 2010; Berckmans et al. 2013), we find that blocking biases are in part associated with mean-state biases, and indeed we also find some improvement with resolution in the simulated mean state of the extratropical atmosphere. Nonetheless, we also show that the agreement between mean-state and blocking biases is far from perfect, illustrating the need for further investigation into the representation of blocking in climate models separate from biases in the mean circulation.

In summary, we show that AGCMs simulate atmospheric blocking more realistically as their grid spacing is reduced to 25 km, yet considerable biases remain also at that resolution. Our results are therefore consistent with previous studies pointing to the importance of model horizontal resolution, which are based on theoretical and numerical studies into the roles of small-scale eddies and orography. At the same time, our results also support previous studies (Jung et al. 2010; Anstey et al. 2013) showing that there are other factors than horizontal resolution limiting the representation of blocking in models.

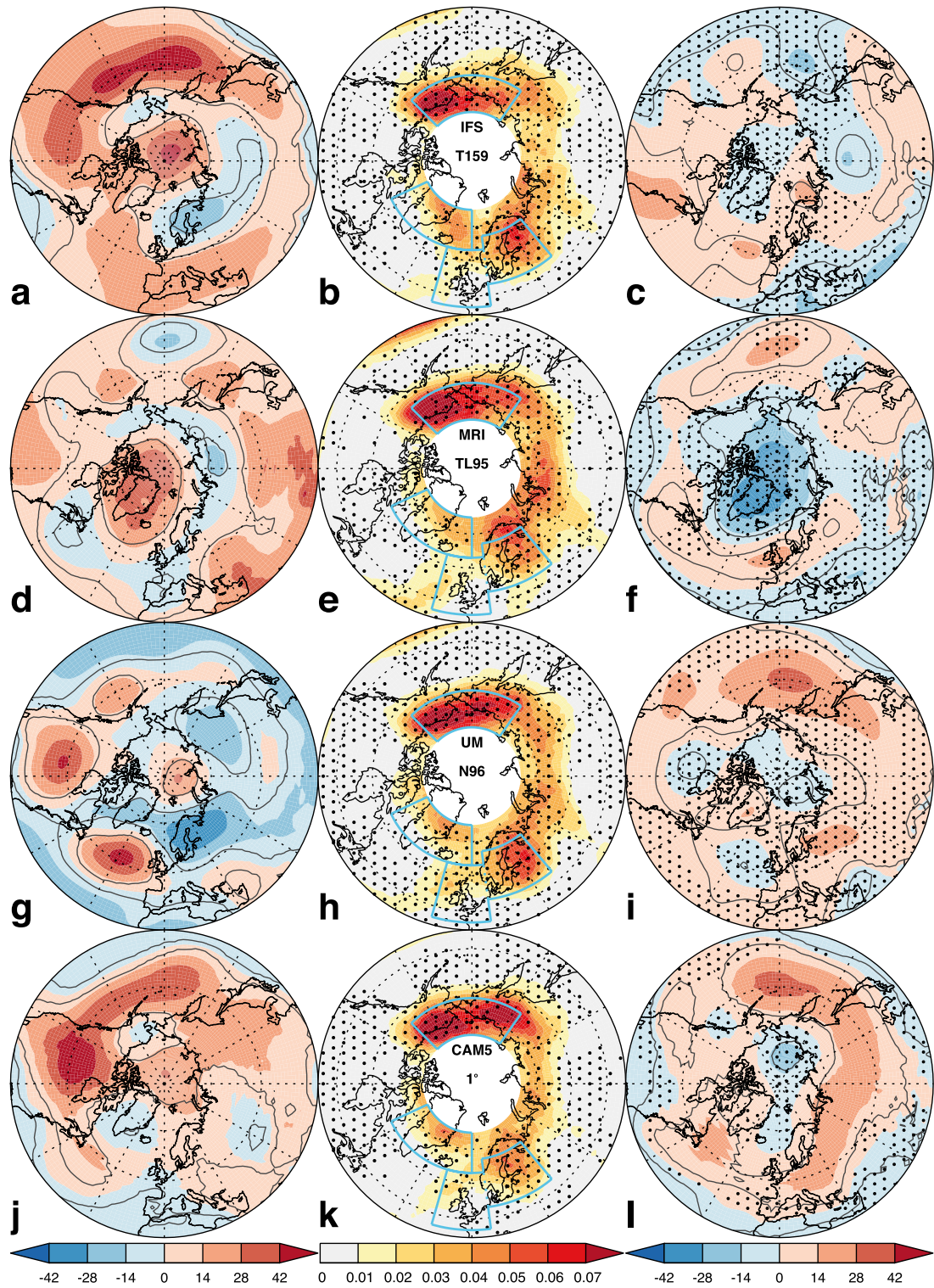


FIG. 15. As in Fig. 13, but for summer (June–August).

Future efforts should include research into (i) how further increases in resolution and the simulation of coupled atmosphere–ocean processes (e.g., Minobe et al. 2008; Hiron et al. 2015) might allow for a more credible simulation of blocking by climate models, the reasons for (ii) the different resolution sensitivity for Atlantic and Pacific blocking, (iii) the seasonality of the sensitivity to resolution over Europe, and (iv) how the model spread in the sensitivity to resolution is related to the structure, physical parameterizations, and numerics of the individual models. The model experiments currently conducted in European Horizon 2020's Process-Based Climate Simulation: Advances in High-Resolution Modeling and European Climate Risk Assessment (PRIMAVERA) and contributing to the High Resolution Model Intercomparison Project (HighResMIP; Haarsma et al. 2016) will offer the possibility to study some of these questions in a well-designed multimodel ensemble of coupled (atmosphere, ocean, sea ice, and land) climate models.

Acknowledgments. RS acknowledges NERC-Met Office JWCRP HRCM funding. PLV, MED, and JS acknowledge NCAS Climate Contract R8/H12/83/001 for the High Resolution Climate Modelling program. PLV (UPSCALE PI) acknowledges the Willis Chair in Climate System Science and Climate Hazards that supports his research. The work of LCS was supported by funding from the European Union's Horizon 2020 research and innovation program under the IMPREX Grant Agreement 641811. MJR and MSM were supported by the Joint U.K. DECC/DEFRA Met Office Hadley Centre Climate Programme (GA01101). We thank the team of model developers and infrastructure experts required to conduct the large UPSCALE simulation campaign and acknowledge use of the MONSooN system, a collaborative facility supplied under the JWCRP; the PRACE infrastructure; the Stuttgart HLRS supercomputing center; and the STFC CEDA service for data storage and analysis using the JASMIN platform. The IFS results described herein were obtained during the 2009/10 Athena Project, a computationally intensive project that was carried out using the Athena supercomputer at the University of Tennessee's National Institute for Computational Sciences (NICS), under the auspices of the National Science Foundation (NSF). Support provided by NICS and the NSF are gratefully acknowledged. The MRI model integrations were performed using the Earth Simulator under the framework of the project "Projection of the Change in Future Weather Extremes using Super-High-Resolution Atmospheric Models" supported by the SOUSEI programs of the Ministry of Education, Culture, Sports, Science and Technology

(MEXT) of Japan. MFW was supported by the Regional and Global Climate Modeling Program of the Office of Biological and Environmental Research in the U.S. Department of Energy Office of Science under Contract DE-AC02-05CH11231. We thank Olivia Romppainen-Martius and Daniela Domeisen for discussion.

REFERENCES

- Anstey, J. A., and Coauthors, 2013: Multi-model analysis of Northern Hemisphere winter blocking: Model biases and the role of resolution. *J. Geophys. Res. Atmos.*, **118**, 3956–3971, doi:10.1002/jgrd.50231.
- Barriopedro, D., R. García-Herrera, and R. M. Trigo, 2010: Application of blocking diagnosis methods to general circulation models. Part I: A novel detection scheme. *Climate Dyn.*, **35**, 1373–1391, doi:10.1007/s00382-010-0767-5.
- , E. M. Fischer, J. Luterbacher, R. M. Trigo, and R. García-Herrera, 2011: The hot summer of 2010: Redrawing the temperature record map of Europe. *Science*, **332**, 220–224, doi:10.1126/science.1201224.
- Berkmans, J., T. Woollings, M.-E. Demory, P.-L. Vidale, and M. Roberts, 2013: Atmospheric blocking in a high resolution climate model: Influences of mean state, orography and eddy forcing. *Atmos. Sci. Lett.*, **14**, 34–40, doi:10.1002/asl2.412.
- Boyle, J. S., 2006: Upper level atmospheric stationary waves in the twentieth century climate of the Intergovernmental Panel on Climate Change simulations. *J. Geophys. Res.*, **111**, D14101, doi:10.1029/2005JD006612.
- Cattiaux, J., R. Vautard, C. Cassou, P. Yiou, V. Masson-Delmotte, and F. Codron, 2010: Winter 2010 in Europe: A cold extreme in a warming climate. *Geophys. Res. Lett.*, **37**, L20704, doi:10.1029/2010GL044613.
- Charney, J. G., and J. G. DeVore, 1979: Multiple flow equilibria in the atmosphere and blocking. *J. Atmos. Sci.*, **36**, 1205–1216, doi:10.1175/1520-0469(1979)036<1205:MFEITA>2.0.CO;2.
- Croci-Maspoli, M., 2005: Climatological investigations of atmospheric blocking: A dynamically-based statistical analysis. Ph.D. thesis, ETH Zürich, 126 pp., doi:10.3929/ethz-a-005062167.
- D'Andrea, F., and Coauthors, 1998: Northern Hemisphere atmospheric blocking as simulated by 15 atmospheric general circulation models in the period 1979–1988. *Climate Dyn.*, **14**, 385–407, doi:10.1007/s003820050230.
- Dee, D. P., and Coauthors, 2011: The ERA-Interim reanalysis: Configuration and performance of the data assimilation system. *Quart. J. Roy. Meteor. Soc.*, **137**, 553–597, doi:10.1002/qj.828.
- Demory, M.-E., P. L. Vidale, M. J. Roberts, P. Berrisford, J. Strachan, R. Schiemann, and M. S. Mizieliński, 2014: The role of horizontal resolution in simulating drivers of the global hydrological cycle. *Climate Dyn.*, **42**, 2201–2225, doi:10.1007/s00382-013-1924-4.
- Doblas-Reyes, F. J., M. A. Pastor, M. J. Casado, and M. Déqué, 2001: Wintertime westward-traveling planetary-scale perturbations over the Euro-Atlantic region. *Climate Dyn.*, **17**, 811–824, doi:10.1007/s003820000146.
- Donlon, C. J., M. Martin, J. Stark, J. Roberts-Jones, E. Fiedler, and W. Wimmer, 2012: The Operational Sea Surface Temperature and Sea Ice Analysis (OSTIA) system. *Remote Sens. Environ.*, **116**, 140–158, doi:10.1016/j.rse.2010.10.017.

- Gates, W. L., 1992: AMIP: The Atmospheric Model Intercomparison Project. *Bull. Amer. Meteor. Soc.*, **73**, 1962–1970, doi:[10.1175/1520-0477\(1992\)073<1962:ATAMIP>2.0.CO;2](https://doi.org/10.1175/1520-0477(1992)073<1962:ATAMIP>2.0.CO;2).
- Haarsma, R. J., and Coauthors, 2016: High Resolution Model Intercomparison Project (HighResMIP). *Geosci. Model Dev.*, **9**, 4185–4208, doi:[10.5194/gmd-9-4185-2016](https://doi.org/10.5194/gmd-9-4185-2016).
- Hirons, L. C., N. P. Klingaman, and S. J. Woolnough, 2015: MetUM-GOML1: A near-globally coupled atmosphere–ocean–mixed-layer model. *Geosci. Model Dev.*, **8**, 363–379, doi:[10.5194/gmd-8-363-2015](https://doi.org/10.5194/gmd-8-363-2015).
- Jung, T., and Coauthors, 2010: The ECMWF model climate: Recent progress through improved physical parametrizations. *Quart. J. Roy. Meteor. Soc.*, **136**, 1145–1160, doi:[10.1002/qj.634](https://doi.org/10.1002/qj.634).
- , and Coauthors, 2012: High-resolution global climate simulations with the ECMWF model in Project Athena: Experimental design, model climate, and seasonal forecast skill. *J. Climate*, **25**, 3155–3172, doi:[10.1175/JCLI-D-11-00265.1](https://doi.org/10.1175/JCLI-D-11-00265.1).
- Kinter, J. L., and Coauthors, 2013: Revolutionizing climate modeling with Project Athena: A multi-institutional, international collaboration. *Bull. Amer. Meteor. Soc.*, **94**, 231–245, doi:[10.1175/BAMS-D-11-00043.1](https://doi.org/10.1175/BAMS-D-11-00043.1).
- Kug, J. S., and F. F. Jin, 2009: Left-hand rule for synoptic eddy feedback on low-frequency flow. *Geophys. Res. Lett.*, **36**, L05709, doi:[10.1029/2008GL036435](https://doi.org/10.1029/2008GL036435).
- Masato, G., B. J. Hoskins, and T. Woollings, 2013: Winter and summer Northern Hemisphere blocking in CMIP5 models. *J. Climate*, **26**, 7044–7059, doi:[10.1175/JCLI-D-12-00466.1](https://doi.org/10.1175/JCLI-D-12-00466.1).
- Matsueda, M., 2011: Predictability of Euro-Russian blocking in summer of 2010. *Geophys. Res. Lett.*, **38**, L06801, doi:[10.1029/2010GL046557](https://doi.org/10.1029/2010GL046557).
- , R. Mizuta, and S. Kusunoki, 2009: Future change in wintertime atmospheric blocking simulated using a 20-km-mesh atmospheric global circulation model. *J. Geophys. Res.*, **114**, D12114, doi:[10.1029/2009JD011919](https://doi.org/10.1029/2009JD011919).
- , H. Endo, and R. Mizuta, 2010: Future change in Southern Hemisphere summertime and wintertime atmospheric blockings simulated using a 20-km-mesh AGCM. *Geophys. Res. Lett.*, **37**, L02803, doi:[10.1029/2009GL041758](https://doi.org/10.1029/2009GL041758).
- Minobe, S., A. Kuwano-Yoshida, N. Komori, S.-P. Xie, and R. J. Small, 2008: Influence of the Gulf Stream on the troposphere. *Nature*, **452**, 206–209, doi:[10.1038/nature06690](https://doi.org/10.1038/nature06690).
- Mizuta, R., and Coauthors, 2012: Climate simulations using MRI-AGCM3.2 with 20-km grid. *J. Meteor. Soc. Japan*, **90A**, 233–258, doi:[10.2151/jmsj.2012-A12](https://doi.org/10.2151/jmsj.2012-A12).
- Neale, R. B., 2012: Description of the NCAR Community Atmosphere Model (CAM 5.0). NCAR Tech. Note NCAR/TN-486+STR, 289 pp. [Available online at http://www.cesm.ucar.edu/models/cesm1.0/cam/docs/description/cam5_desc.pdf.]
- Otto, F. E. L., N. Massey, G. J. Van Oldenborgh, R. G. Jones, and M. R. Allen, 2012: Reconciling two approaches to attribution of the 2010 Russian heat wave. *Geophys. Res. Lett.*, **39**, L04702, doi:[10.1029/2011GL050422](https://doi.org/10.1029/2011GL050422).
- Rayner, N. A., D. E. Parker, E. B. Horton, C. K. Folland, L. V. Alexander, D. P. Rowell, E. C. Kent, and A. Kaplan, 2003: Global analyses of sea surface temperature, sea ice, and night marine air temperature since the late nineteenth century. *J. Geophys. Res.*, **108**, 4407, doi:[10.1029/2002JD002670](https://doi.org/10.1029/2002JD002670).
- Rex, D. F., 1950: Blocking action in the middle troposphere and its effect upon regional climate. *Tellus*, **2A**, 275–301, doi:[10.1111/j.2153-3490.1950.tb00339.x](https://doi.org/10.1111/j.2153-3490.1950.tb00339.x).
- Reynolds, R. W., N. A. Rayner, T. M. Smith, D. C. Stokes, and W. Wang, 2002: An improved in situ and satellite SST analysis for climate. *J. Climate*, **15**, 1609–1625, doi:[10.1175/1520-0442\(2002\)015<1609:AHASAS>2.0.CO;2](https://doi.org/10.1175/1520-0442(2002)015<1609:AHASAS>2.0.CO;2).
- Rienecker, M. M., and Coauthors, 2011: MERRA: NASA's Modern-Era Retrospective Analysis for Research and Applications. *J. Climate*, **24**, 3624–3648, doi:[10.1175/JCLI-D-11-00015.1](https://doi.org/10.1175/JCLI-D-11-00015.1).
- Scaife, A. A., T. Woollings, J. Knight, G. Martin, and T. Hinton, 2010: Atmospheric blocking and mean biases in climate models. *J. Climate*, **23**, 6143–6152, doi:[10.1175/2010JCLI3728.1](https://doi.org/10.1175/2010JCLI3728.1).
- Scherrer, S. C., M. Croci-Maspoli, C. Schwiertz, and C. Appenzeller, 2006: Two-dimensional indices of atmospheric blocking and their statistical relationship with winter climate patterns in the Euro-Atlantic region. *Int. J. Climatol.*, **26**, 233–249, doi:[10.1002/joc.1250](https://doi.org/10.1002/joc.1250).
- Shutts, G. J., 1983: The propagation of eddies in diffluent jetstreams: Eddy vorticity forcing of 'blocking' flow fields. *Quart. J. Roy. Meteor. Soc.*, **109**, 737–761, doi:[10.1002/qj.49710946204](https://doi.org/10.1002/qj.49710946204).
- , 1986: A case study of eddy forcing during an Atlantic blocking episode. *Advances in Geophysics*, Vol. 29, Elsevier, 135–162, doi:[10.1016/S0065-2687\(08\)60037-0](https://doi.org/10.1016/S0065-2687(08)60037-0).
- Tibaldi, S., and F. Molteni, 1990: On the operational predictability of blocking. *Tellus*, **42A**, 343–365, doi:[10.1034/j.1600-0870.1990.t01-2-00003.x](https://doi.org/10.1034/j.1600-0870.1990.t01-2-00003.x).
- , E. Tosi, A. Navarra, and L. Pedulli, 1994: Northern and Southern Hemisphere seasonal variability of blocking frequency and predictability. *Mon. Wea. Rev.*, **122**, 1971–2003, doi:[10.1175/1520-0493\(1994\)122<1971:NASHSV>2.0.CO;2](https://doi.org/10.1175/1520-0493(1994)122<1971:NASHSV>2.0.CO;2).
- Uppala, S. M., and Coauthors, 2005: The ERA-40 re-analysis. *Quart. J. Roy. Meteor. Soc.*, **131**, 2961–3012, doi:[10.1256/qj.04.176](https://doi.org/10.1256/qj.04.176).
- Walters, D. N., and Coauthors, 2011: The Met Office Unified Model Global Atmosphere 3.0/3.1 and JULES Global Land 3.0/3.1 configurations. *Geosci. Model Dev.*, **4**, 919–941, doi:[10.5194/gmd-4-919-2011](https://doi.org/10.5194/gmd-4-919-2011).
- Woollings, T., 2010: Dynamical influences on European climate: An uncertain future. *Philos. Trans. Roy. Soc. London*, **368A**, 3733–3756, doi:[10.1098/rsta.2010.0040](https://doi.org/10.1098/rsta.2010.0040).
- , A. Hannachi, and B. Hoskins, 2010: Variability of the North Atlantic eddy-driven jet stream. *Quart. J. Roy. Meteor. Soc.*, **136**, 856–868, doi:[10.1002/qj.625](https://doi.org/10.1002/qj.625).
- Zappa, G., L. C. Shaffrey, and K. I. Hodges, 2013: The ability of CMIP5 models to simulate North Atlantic extratropical cyclones. *J. Climate*, **26**, 5379–5396, doi:[10.1175/JCLI-D-12-00501.1](https://doi.org/10.1175/JCLI-D-12-00501.1).
- , G. Masato, L. Shaffrey, T. Woollings, and K. Hodges, 2014: Linking Northern Hemisphere blocking and storm track biases in the CMIP5 climate models. *Geophys. Res. Lett.*, **41**, 135–139, doi:[10.1002/2013GL058480](https://doi.org/10.1002/2013GL058480).